REVISTA SOLDAGEM & INSPEÇÃO

ISSN 1980-6973 (Online) | ISSN 0104-9224 (Print)

ORIGINAL ARTICLE

Microstructure, Mechanical and Corrosion Behavior of Friction Stir Processed AA6082 with Cr_3C_2 Particles

Rajarajan Bharathikanna[1], Govindaraj Elatharasan[2]

[1] Nehru Institute of Technology, Department of Mechanical Engineering, Coimbatore, Tamilnadu, India.
[2] University College of Engineering, Department of Mechanical Engineering, Rajamadam Campus, Pattukottai, Tamilnadu, India.

How to cite: Bharathikanna R, Elatharasan G. Microstructure, mechanical and corrosion behavior of friction stir processed AA6082 with Cr3C2 particles. Soldagem & Inspeção. 2022;27:e2723. https://doi.org/10.1590/0104-9224/SI27.23.

Abstract: Friction stir processing (FSP) is a novel method of metal surface modification during the process by the addition of strengthening particles. FSP produced refined microstructures with the development of added ceramic particles on surface metal. In this FSP, mechanical characteristics were enhanced by FSP parameters, tool spinning speed, traverse speed and the axial force of high carbon high chromium die steel (non-consumable tool). In this research, FSP technique was employed on the surface of the base metal AA6082 aluminium alloy to modify composites of metal surface utilizing Cr_3C_2 particles. Mechanical properties like tensile strength, processed surface hardness and microstructure were studied. This research mainly focused on the parametric optimization of FSP on AA6082 with multiple responses (tensile strength and processed surface hardness) based on Taguchi L9 orthogonal array and grey relational analysis (GRA). The significant FSP parameters were obtained by grey relational grade (GRG) with an analysis of variance tool. Axial force and traverse speed were the most significant FSP parameters, which the most influence of performance characteristic of friction stir processed specimens. The predicted values were validated by confirmation test at setting of optimum level exhibits better conformity with investigational values. Field Emission Scanning Electron Microscope (FESEM) was carried out to determine the presence of strengthening particles in the processed Aluminium alloy.

Key-words: FSP; Cr_3C_2; GRA; FESEM.

1. Introduction

Materials are the pivotal element in any manufacturing process which has to be carefully selected in the product development phase for the success of the product to be launched in the market. The material selection process involves many criteria's which has to be carefully considered to avoid early stage mistakes which may be the root cause for a bigger failure. The microstructure of a material has a very strong influence over the physical properties such as strength, toughness, hardness, corrosion resistance and many more. The modification of material microstructure can bring many potential advantages in diverse applications. Different techniques have been adopted by industrialists and researchers for modifying the microstructure of a material to make them suitable for a particular application. Friction Stir Processing (FSP) is a promising technique for the grain refinement of materials which has its root from Friction Stir Welding (FSW) technology. Owing to its positive benefits such as enhanced mechanical properties, less distortion, reduced residual stresses and good quality joints this technique has a wide adoption with materials such as aluminium alloys, magnesium alloys, titanium alloys, copper-zinc alloys and metal matrix composites. The general theory of FSP is extremely uncomplicated. Because, this FSP follow the principle of the FSW and it is a solid state process, initially advanced for aluminium alloys. It is raising technique for employing with metals that can present localized improvement and manage of microstructures in nearby processed materials of surface layers [1-3]. Mostafa Dadaei et al. [4] considered both Aluminium oxide and silicon carbide nano particulates which were added on the alloy surface to modify the base metal characteristics. FSP produced better mechanical characteristics by added both the particles. In this research, tensile and yield properties were found by the researchers. The outcomes exhibited that the processing has changed the grain size. Both the strengthen particles were improved the base metal surface during FSP. Finally, the researchers reported that the silicon carbide composition is more advantageous than aluminium oxide. Similarly, the SiC distributed over the surface of the processed specimen. Chanakyan et al. [5] applied the grey relational analysis and Taguchi method on AA2024 and AA6061 through the FSW. The authors have studied the impact of various tool pin diameter, weld speed, and spinning speed during the welding process and found that both welding speed, tool spinning speed were the most significant FSW parameter affecting the output parameters. Elatharasan et al. [6] developed the statistical model of FSW process parameters for the materials AA6061 and AA5083 through grey relational analysis. They obtained high quality welds of FSW on the dissimilar alloy by adopting optimum process parameters. The authors have predicted the optimum FSW parameters by using the multi-objective method. ANOVA was used for the confirmation level. The microstructure analysis revealed some defects

Received: 20 June 2021. Accepted: 28 Aug., 2022.
E-mails: bharathikanna89@gmail.com (RB), gelatharasan@gmail.com (GE)

produced during FSW. Sachin Jambhale et al. [7] studied the friction stir spot welded joint of AA6082 and AA6061. The following parameters, namely, pin profile, dwell time, tool tilt angle, and tool rotation speed, were investigated. Taguchi's orthogonal array method analyzed two responses, such as shear strength and hardness. An analysis of variance was also executed for those two responses. The optimal arrangements of FSP parameters were successfully obtained through grey relational method. Sahu et al. [8] exploited the benefits of grey relational analysis method for FSWed magnesium alloy. This investigation optimized the FSW parameters to compose the good mechanical strength of the welded base metal. The Taguchi L_{18} array was used for their experiments, and its rankings were indicated for optimized parameters. ANOVA technique has been adopted for identifying the significant and insignificant process parameters affecting the outputs. Sudhagar et al. [9] made an attempt on AA2024 alloy by the FSW method for selecting the optimal parameters. The experiments were conducted with Taguchi L9 array and the experimental data was analyzed using grey relational analysis. As input parameters the authors used tool offset, welding speed, and tool spinning speed, and the welded responses hardness, toughness, and tensile strength were considered as output. The grey relational analysis and ranking order techniques were used to find the optimal FSW parameters, maximizing the output responses. N. Wakchaure et al. [10] developed the grey relation technique and artificial neural network to optimize the FSW parameters with AA 6082 alloy responses. The selected FSW parameters were tool tilt angle, traverse speed and spinning speeds, and L_{27} Orthogonal array (Full Factorial) has been used for creating the experimental layout. Finally, the optimal FSW parameters and newly made tools were developed by artificial neural networks with Taguchi-related grey relational analysis. Due to the multi-objective method, the characteristics of welded metals were improved. Arun Babu et al. [11] performed FSW for evaluating the post weld characteristics of AA 7075. The authors focused on process parameters such as shoulder diameter, tool tilt angle, traverse speed, rotational tool speed on output response (tensile strength) by varying 6% wt in base metal with tungsten carbide in AA7075. An approach of Taguchi design measured the optimal process parameters. The tool pin profile, traverse, and tool rotation speed were the most preferential parameters of welded joint tensile quality. Chanakyan and Sivasankar [12] studied the numerical method on friction stir processing through the design of experiments. The authors have created the experimental design matrix through DOE methods such as Central composite design and Box Behnken method for obtaining the output with enhanced quality in multi variable problems. The authors have demonstrated the capabilities of Artificial Neural Network and other related techniques. The authors have concluded FSP as a promising technique for developing composites. Mahmoud et al. [13] processed silicon carbide particulate applied over the surface of AA1050 base metal. They investigated the impacts of tool spinning speed, no. of. FSP passes, traverse speed based on the grooved position. The authors have reported that the composites with silicon carbide composites have shown superior mechanical performance. Dinaharan et al. [14] investigated the effect of reinforcement particles such as carbides of silicon, tungsten, titanium and aluminium oxide with base metal AA6082 alloy. The authors have prepared samples by processing through FSP technique for analyzing the microstructure and measuring the UTS of final composite material developed. The authors have indicated that the presence of such reinforcement particles has shown little influence over microstructure and UTS. Barati et al. [15] conducted the corrosion and mechanical test on the friction stir processed AA6082 with silicon carbide composites through the vibration technique. The mechanical properties were improved at FSPed specimens and the corrosion resistances were improved by 78 percent due to the presence of surface composites. Mahajan et al. [16] processed the chromium carbide with magnesium alloy by the route of reduction technique and its end product is thermally sustained with aluminium alloy and also optimized with GRG. Yang et al. [17] analyzed grain structure resulted from antioxidant process between aluminium alloy and chromium carbide. Sahu et al. [18] studied the microstructure analysis among the chromium carbide and aluminium alloy by heat treatment method and studied the grain structure of chromium carbide. The above reference [16] to [18] indicatesthat the addition of chromium carbide with aluminium alloy has resulted in a great improvement in various mechanical properties studied.

From the literature survey carried out, it is understood that the addition of Cr_3C_2 is a better surface reinforcement element for applying over the base metal alloy AA6082.The current study focus upon the identification of optimal process parameters through Taguchi's Orthogonal Array and Grey Relational Analysis which enhances tensile strength and corrosion behavior of the resulting specimen.

2. Experimentation

AA6082 is the base metal utilized in fabrication of top surface composites composed by FSP method for this investigation. The base plate is slash into measurements having 99 mm length; 99.5 mm width and 6 mm thickness prepared with 6 holes that were drilled in the center of the specimen having the dimensions of 3mm depth and 3 mm diameter. The center to center distance of drilled holes is 16.33 mm. Each hole was filled with Cr_3C_2 particles with size of 20 micro meters. A high carbon high chromium tool material is used in this FSP technique. In this investigation, the high carbon high chromium die steel tool is plunged into the base metal, and it's rotated and stirred through the base metal thickness. First, the particles were packed by pin less tool. Second, the straight threaded cylinder tool pin profile fabricates the FSP runs. The straight threaded cylinder tool dimensions had 18 mm of shoulder diameter and 5.7 mm of pin length, respectively [19]. The weight percentage of AA 6082 chemical compositions and its properties is presented in Table 1 and 2 respectively. Based on L9 orthogonal array, 9 processing runs were performed by FSP with FSW machine. The Figure 1 shows the experimental work plan. Figures 2 and 3 shows the configuration of AA6082 before processing and friction stir processed specimen, respectively.

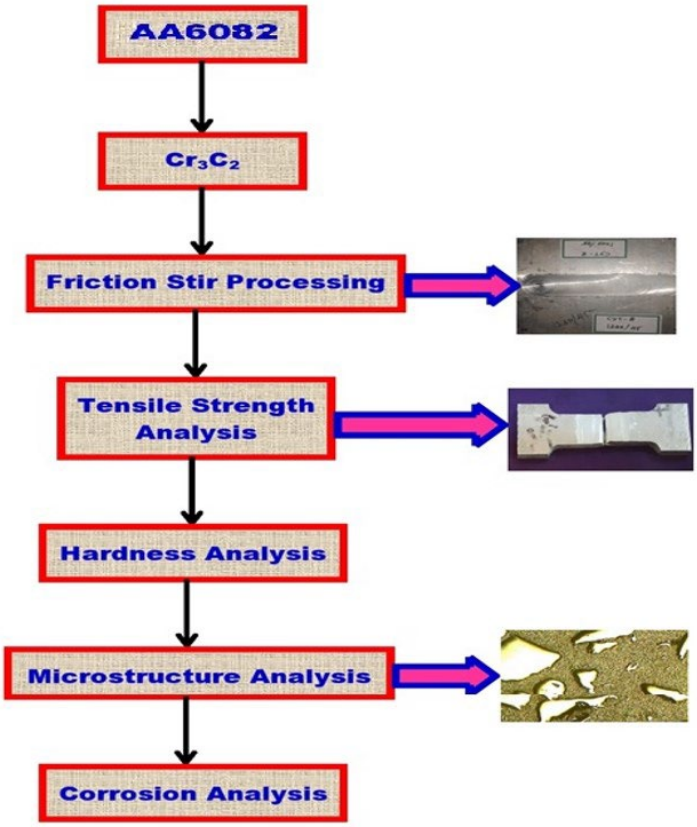

Figure 1. Experimental Work Plan

Table 1. AA 6082 chemical composition.

Portion	Al	Si	Mg	Cr	Ti	Zn	Mn	Cu	Fe
Weight in %	Bal	0.7	0.6	0.2	0.1	0.1	0.5	0.1	0.3

Table 2. AA 6082 mechanical properties.

Tensile strength (MPa)	% of elongation	Micro hardness (Hv)
231	10	60

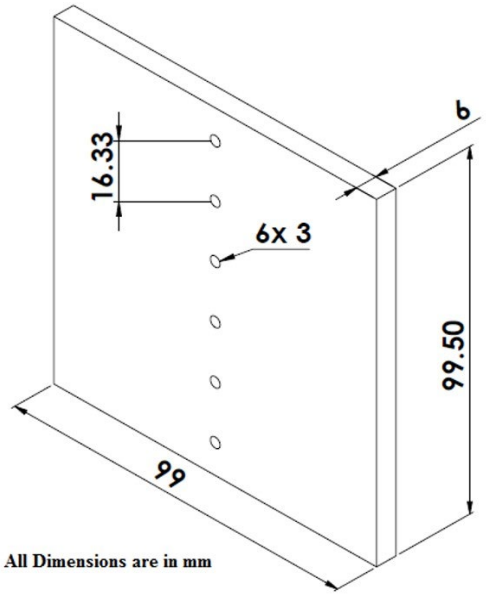

Figure 2. Configuration of AA6082 specimen.

Figure 3. Friction stir processed AA6082 and Cr_3C_2

In this present study, process parameters of FSP such as tool spinning speed, weld or traverse speed and axial force were considered as input parameters to evaluate their influence over the output responses. The three parameters and the three level factorial plans designed by Taguchi L_9 orthogonal array are exhibited in Tables 3 and 4 respectively.

Table 3. FSP parameters and its level of factors.

FSP	SYMBOL	S.I Unit	LEVELS		
			1	2	3
Rotational Speed	RTS	(rpm)	800	1000	1200
Traverse Speed	TSS	(mm/min)	30	45	60
Axial Load	AL	(kN)	5	6	7

Table 4. Taguchi L_9 orthogonal array for FSP.

FSP	Rotational Speed – rpm (RTS)	Traverse Speed - mm/min (TSS)	Axial Load – kN (AL)
1	800	30	5
2	800	45	6
3	800	60	7
4	1000	30	6
5	1000	45	7
6	1000	60	5
7	1200	30	7
8	1200	45	5
9	1200	60	6

3. Results and Discussion

This section is focused to provide an output for modified surface properties with influence of different FSP parameters by Taguchi. Optimal parameters were successfully identified with GRG analysis from the mechanical behaviors like tensile and microhardness. Optical microstructures, FESEM with EDS analysis and corrosion test were conducted on the lower and higher optimal specimens. Experimental investigations are well discussed in the following categories.

3.1. Grey relational formation

Grey relational formation is expressed as preprocessing the information (data), which correlates to a group of series (sequence). Based on essential standards, standardization of experimental outputs attained for responses is completed. In the friction stir processed specimen, the maximum value of tensile strength (TS) and processed surface hardness (PSH) is preferred. The TS and PSH are the output responses computed by the grey relational grade. In the present study, the Larger the better method is used to focus the maximum objective function from the output responses and it is also measured to optimize output response (TS and PSH). Equation 1 is used for calculating the standardized values of response in Larger the better condition.

$$x_i(p) = \frac{y_i(p) - \min y_i(p)}{\max y_i(p) - \min y_i(p)} \quad (1)$$

Where p= 1, 2, 3,…., n; i= 1, 2, 3,…., m; m = no. of. Investigational data, n = no. of. Factors, x_i is the value attained after grey relational formation. The $\min y_i(p)$ is the minimum value of $y_i(p)$ and $\max y_i(p)$ is the maximum value of $y_i(p)$.

3.2. Grey relational coefficient

Equation 2 is utilized for computing the grey relational coefficient (GRC).

$$\zeta i(p) = \frac{\Delta_{min} + ¥\Delta_{max}}{\Delta_{0i}(p) + ¥\Delta_{max}} \quad (2)$$

Where $\zeta i(p)$ is the grey relational coefficient of ithrun for the pth response. $\Delta_{0i}(p)$is sequence of deviation between $x_0(p)$ and $x_i(p)$. Here, $x_0(p)$ is a sequence of ideal reference. ¥ is the coefficient of distinguishing and set constant value at 0.5.

3.3. Computing techniques of grey relational grade

The grey relational grade is computed by using Equation 3. The GRG is mainly computed from the average of grey relational coefficient related to responses (TS and PSH). The complete performance character of the responses mainly depends upon the grey relational grade [20,21].

$$y_i = \sum_{k=1}^{n} w_i \zeta_i(p) \quad (3)$$

Where y_i is the grey relational grade for ith run (experiment). The maximum value of GRG intimates the nearness of experiment correlated with standardized value.

3.4. Tensile strength and surface hardness

As per L_9 Taguchi orthogonal array, 9 experimental specimens were prepared by FSP technique. Tensile strength is one of the mechanical property indexes for parts made using the FSP process. The tensile strength (TS) of friction stir processed AA6082 material depends on various process parameters namely tool spinning speed, weld speed and axial force. As per standard of ASTM-E9 tensile trials were arranged from each friction stir processed samples and investigated in Universal testing machine. The tensile test specimens were cut from friction stir processed samples perpendicularly to process direction and arranged to carry out the tensile strength. In this study, microhardness tests (Vickers's) were utilized to illustrate the hardness of AA 6082 parent metal and friction stir processed zones (Parent metal, Heat affected zone, Thermo-mechanically affected zone and Nugget Zone). The micro hardness inspections were performed on friction stir processed region in the middle-segment of all the experiments using Vickers hardness equipment. The computed values of TS and PSH with standardized values of GRA are presented in Table 5. Photograph of fractured tensile samples were shown in Figure 4. The graphs of tensile and Vickers's hardness outcomes were exhibited in Figures 5 and 6 respectively.

Figure 4. Fractured tensile samples of AA6082 and Cr_3C_2

Table 5. Experimental and Standardized values of GRA.

FSP	Experimental		Standardized	
	TS (MPa)	PSH (Hv)	TS (MPa)	PSH (Hv)
1	148.74	82.054	0.729	0.673
2	172.02	85.05	0.994	0.804
3	113.94	71.632	0.334	0.215
4	114.23	66.728	0.337	0.000
5	103.26	70.408	0.213	0.162
6	158.37	87.99	0.839	0.934
7	84.54	74.692	0.000	0.350
8	172.55	89.504	1.000	1.000
9	101.66	79.002	0.195	0.539

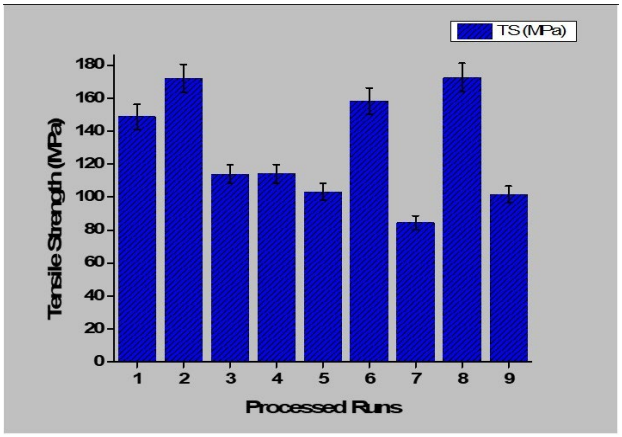

Figure 5. Tensile Results with FSP Runs.

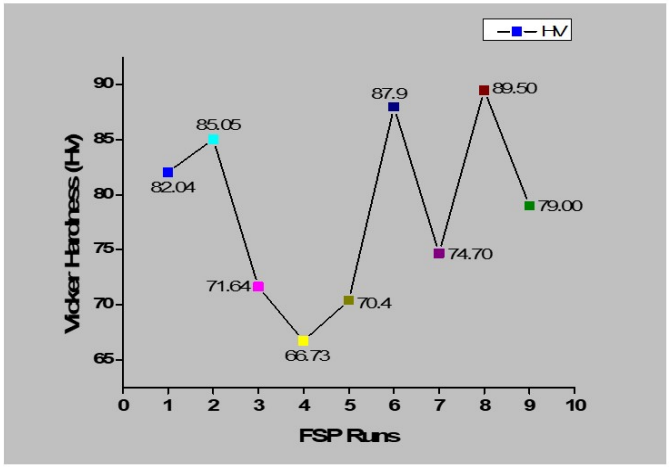

Figure 6. Vickers's Hardness Results with FSP Runs.

3.5. Computation of GRG, Mean of S/N ratio and GRG

The Equation 3 which represents the Grey Relational Grade (GRG) has been adopted for calculating the GRG values of output responses (TS and PSH). The sequence group, grey relational coefficient, grey relational grade and its rank values are displayed in Table 6. For calculating the grey relational grade, equal weight of 0.5 is allotted to both TS and PSH. The overall multi responses performance was computed by grey relational grade. After getting the maximum GRG value, the three level GRG mean was tabulated with three FSP parameters exhibited in Table 7. Optimum parameters value of processed specimen was indicated in the order of axial load, traverse speed and rotational speed at the level 3-2-1. The signal to noise ratio (S/N) and GRG mean values were calculated for the experimental output values to obtain the combination of parameter setting which can enhance output characteristics to the desired or optimum level. Larger the better solution is chosen for signal to noise ratio to maximize the output responses values and the results are in Table 8.The mean of the S/N ratio and GRG at three levels of FSP are exhibited in Table 9. The greatest value of GRG mean was attained at the 1st level of axial load 5 kN, 2nd level of traverse speed 45 mm/min, and 1st level of tool rotational speed 800 rpm, respectively. The mean response of the greater GRG was the most preferential level suggested by the S/N ratio for FSP.

Table 6. Analysis of sequence, GRC, GRG and its rank.

FSP	Sequence		Grey relational coefficient		Grey Relational Grade	Rank
	TS (MPa)	PSH (Hv)	TS (MPa)	PSH (Hv)		
1	0.271	0.327	0.649	0.605	0.6267103	4
2	0.006	0.196	0.988	0.719	0.8534739	2
3	0.666	0.785	0.429	0.389	0.4090181	6
4	0.663	1.000	0.430	0.333	0.3816923	8
5	0.787	0.838	0.388	0.374	0.3809919	9
6	0.161	0.066	0.756	0.883	0.8194742	3
7	1.000	0.650	0.333	0.435	0.3839949	7
8	0.000	0.000	1.000	1.000	1.0000000	1
9	0.805	0.461	0.383	0.520	0.4516197	5

Table 7. Response tables for GRG at 3 levels.

FSP	GRG-LEVELS			Rank
	1	2	3	
RTS	0.6297	0.4641	0.8154	3
TSS	0.5274	0.7448	0.5623	2
AL	0.6119	0.5600	0.3913	1

Table 8. Mean of grey relational grade and S/N ratio.

FSP	RTS (rpm)	TSS (mm/min)	AL (kN)	Mean of GRG	S/N Ratio
1	800	30	5	0.6267103	-4.05866
2	800	45	6	0.8534739	-1.37619
3	800	60	7	0.4090181	-7.76515
4	1000	30	6	0.3816923	-8.36573
5	1000	45	7	0.3809919	-8.38169
6	1000	60	5	0.8194742	-1.72929
7	1200	30	7	0.3839949	-8.31349
8	1200	45	5	1.0000000	0.00000
9	1200	60	6	0.4516197	-6.90454

Table 9. S/N ratio and GRG mean at 3 level.

Level	For S/N Ratio			For GRG Mean		
	RTS(rpm)	TSS(mm/min)	AL (kN)	RTS(rpm)	TSS(mm/min)	AL (kN)
1	-4.400	-6.913	-1.929	0.6297	0.4641	0.8154
2	-6.159	-3.253	-5.549	0.5274	0.7448	0.5623
3	-5.073	-5.466	-8.153	0.6119	0.5600	0.3913
(Delta)	0.1023	0.2807	0.4241	1.759	3.660	6.224
(Rank)	3	2	1	3	2	1

3.6. ANOVA for GRG

The tool ANOVA helps to identify the significant parameters of FSP, which influence the grey relational analysis. In present studies, the ANOVA is utilized to categorize the noteworthy FSP parameters incorporated with processed specimens. From Table 9, optimized FSP parameters are 3-2-1, which is axial load 5 kN, traverse speed 45 mm/min, and tool rotational speed 800 rpm. Delta indicates the difference between the responses of higher and lower values. The rank order shows the order of significance, which exhibits axial load (AL) as necessary as the other two FSP parameters, followed by traverse speed and tool rotational speed. Figures 7 to 12 displays the GRG means, and S/N ratio means for FSP parameters is utilized to identify the effect of each input factor. The plots suggest that the GRG responses (TS and PSH) increase as RTS and TS increase. The ANOVA results are displayed in Table 10. The 95% confidence level was maintained for calculating the p-value. The FSP parameters AL and TSS are more significant than RTS. The axial load attained a maximum of 66.1% contribution, higher than that of other parameters. Traverse and rotational speed contributed 29.5 and 4.3%, respectively [22].

Table 10. ANOVA for GRG output.

Parameters	DOF	Seq (SS)	Adj (SS)	Adj(MS)	F Value	P Value	% Contribution
RTS (rpm)	2	0.01793	0.01793	0.008966	0.30	0.06	4.3%
TSS (mm/min)	2	0.12213	0.12213	0.061065	2.04	0.03	29.5%
AL (kN)	2	0.27312	0.27312	0.136560	4.57	0.01	66.1%
Error	2	0.05976	0.05976	0.029881			0.1%
Total	8	0.47294					100%
S= 0.1729 ; R-sq (adj) = 87.4% ; R-Sq = 86.4%							

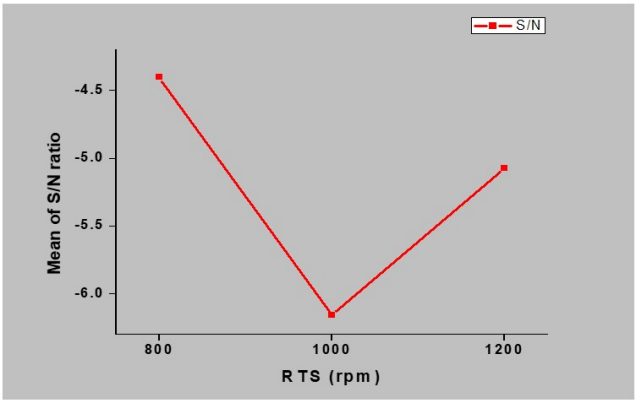

Figure 7. RTS (Rotational speed-rpm) and S/N Ratio Mean.

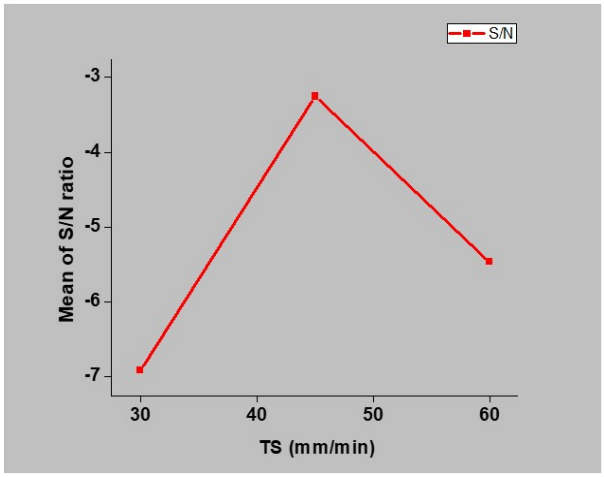

Figure 8. TSS (Traverse speed-mm/min) and S/N ratio Mean.

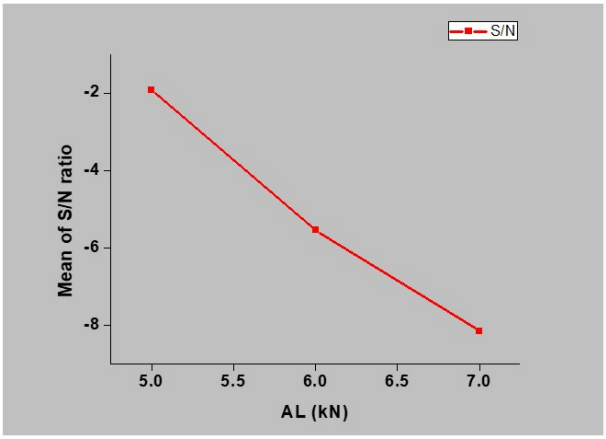

Figure 9. AL (Axial load- kN) and S/N ratio Mean.

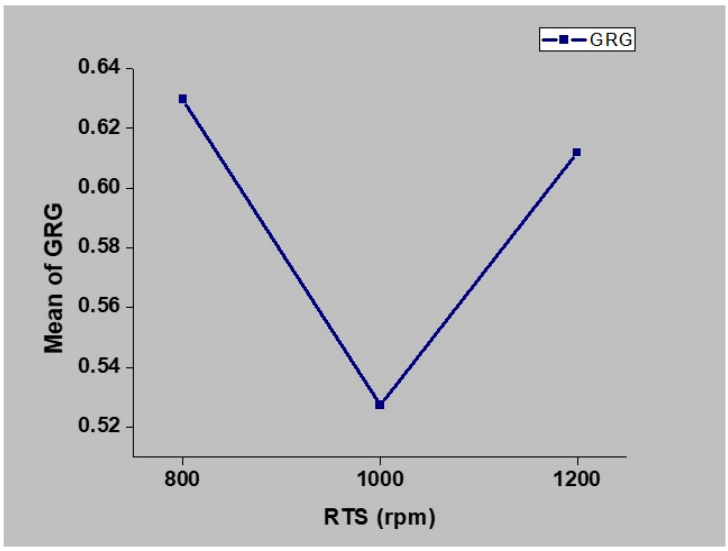

Figure 10. RTS (Rotational speed-rpm) and GRG Mean.

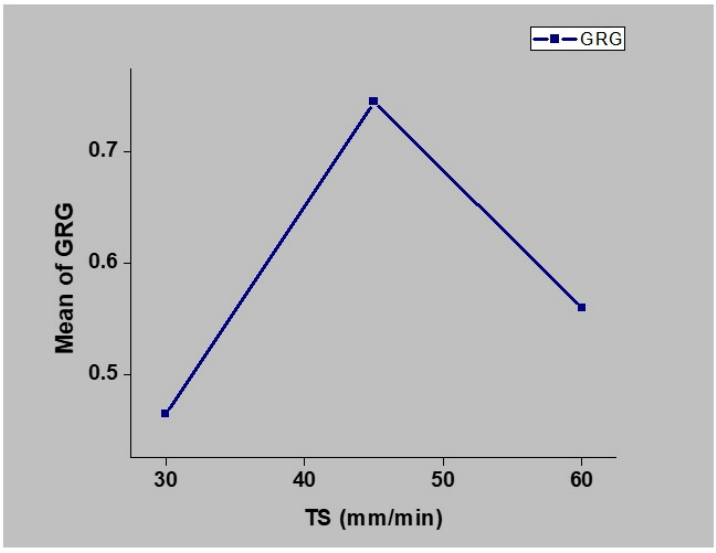

Figure 11. TSS (Traverse |speed-mm/min) and GRG Mean

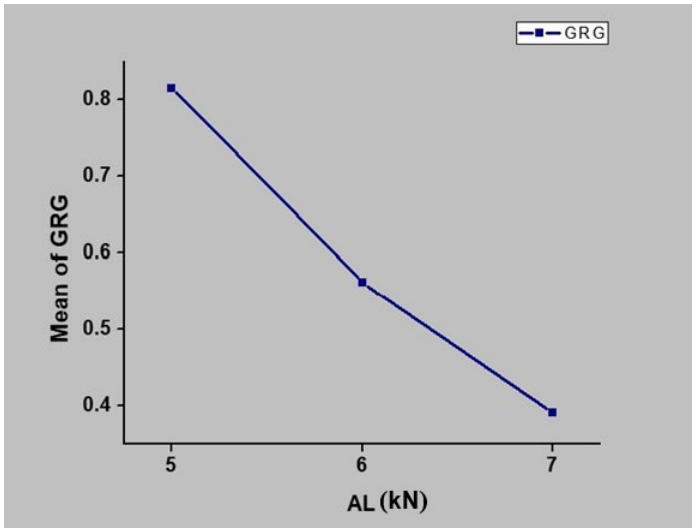

Figure 12. AL (Axial load- kN) and GRG Mean.

3.7. Contour plots for GRG with FSP parameters

The Figures 13 to 15 shows contour analysis for GRG mean with effect of FSP parameters. The Figure 13 exhibits that better GRG value was attained at traverse speed (TS) of 45 mm/min and at rotational speed (RTS) of 1200 rpm. The Figure 14 displays that superior GRG value was attained at traverse speed (TS) of 45 mm/min and axial load (AL) of 5 kN. The Figure 15 shows that higher GRG value was obtained at axial load (AL) of 5 kN and rotational speed (RTS) of 1200 rpm. The contour plots created highlights that the FSP parameter axial load has more significance than other parameters considered.

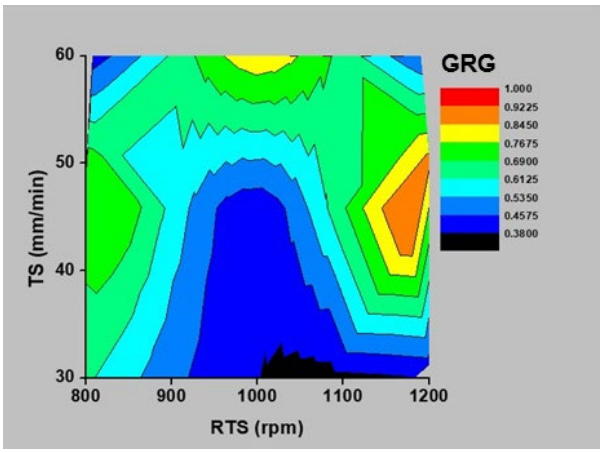

Figure 13. RTS (Rotational speed-rpm) and TSS (Traverse speed-mm/min) with GRG.

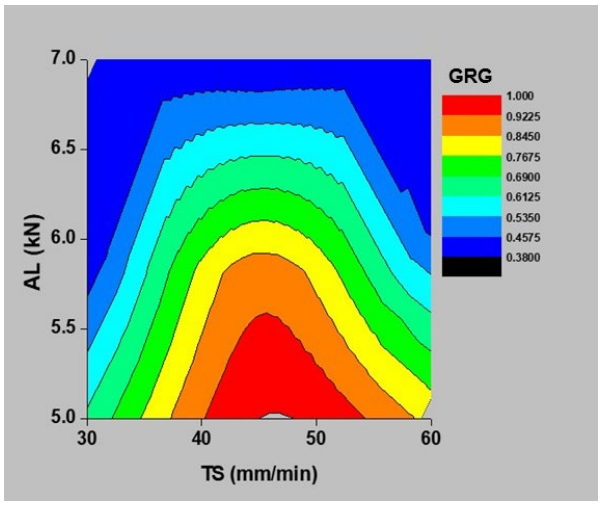

Figure 14. TSS (Traverse speed-mm/min) and AL (Axial load-kN) with GRG.

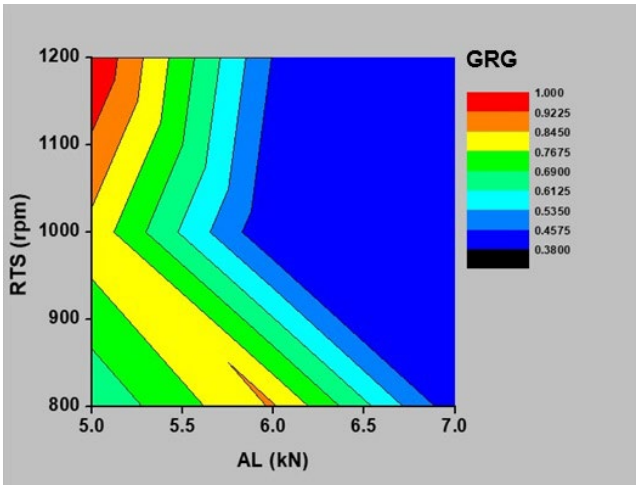

Figure 15. AL (Axial load-kN) and RTS (Rotational speed-rpm) with GRG.

3.8. Validation test using optimum level of process parameters

The validation of output parameters has been done using the optimum level of parameter settings obtained from grey relational analysis. Equation 4 represents the relationship existing between the output parameter and input parameters used in the current study. The term $\hat{y}$ denotes the estimated output parameter from the input variables.

$$\hat{y} = y_m + \sum_{i=1}^{q}(\overline{y_i} - y_m) \quad (4)$$

Where y_i and y_m is the GRG and overall mean at the optimized level. The multiple performances attributes performed by the number of FSP parameters is indicated by (q). The function of the total GRG is utilized to convert a process of multi-response into single response optimal condition. The investigational and predicted values are computed by Equation 4 and presented in Table 11. The optimal FSP parameters are 1200 rpm RTS, 45 mm/min TSS and 5 kN AL. The verification tests were carried out with optimized FSP parameters. The GRG values of initial and optimal parameter settings are in close agreement with each other by having actual value as 0.990 and the predicted value is 0.995. The measured values of tensile strength and micro hardness are found to be in good accordance with less error percentage.

Table 11. Validation Test of FSP with GRA.

Original Processing Parameters	Original Levels of Processing Parameters	Optimal FSP Parameter using GRA
Factor Level	RTS-3, TSS-2, AL-1	RTS-1, TSS-2, AL-1
Tensile Strength(Mpa)	172.55	175.98
Micro Hardness-Hv	89.504	91.254
Grey relational grade	0.990	0.995

3.9. Microstructure analysis of optimum processed specimen

The microstructures of friction stir processed with optimal parameters which are based on the rank orders specimens were conducted using the optical microscope to examine the coarse grain changes from base metal to stirred zones (processed with Cr_3C_2). The ranking of experimental trials have been considered for selecting the workpieces for microstructural evaluation. The specimens ranked with numbers such as 1, 3 6 and 9 have been selected for further processing. As per GRG values , specimen prepared from experimental trail 8 ranks top , specimens 6 ranks 3rd position , specimen 3 ranks 6th position and 5th specimen takes the last position. The selected specimens are sliced and subsequently engraved, buffed with Keller's reagent solution.

All the processed zones show the changes of fine grain structure with intermetallic compounds (AA6082 and Cr_3C_2 particulate). The micrographs of processed specimens were taken on the heat affected zones and nugget zones. During the FSP, Cr_3C_2 particles were distributed evenly in stirred zone (processed zone) due to the optimal parameters. So that, the distributions of grains is processed at various locations of localized area (Processed area). The HAZ exhibits microstructure with grains which have increasing size and possess slight similarity with the parent material due to low temperature processing conditions. The rank 1 processed specimen of stirred zone exhibits fine grains having no clustering of intermetallic compounds, due to the higher rotational speed with intermediate traverse speed. The stirred zone micrographs of rank 1 with lower and higher magnification are presented in Figure 16. The HAZ micrograph of the rank 1 specimen is exhibited in the Figure 17. The rank 3 processed specimen of stirred zone displays the fine grains having low clustering of intermetallic compounds produced, due to the higher traverse speed and intermediate rotational speed. The stirred zone micrographs of rank 3 with lower and higher magnification are indicated in Figure 18. The HAZ micrograph of the rank 3 specimen is displayed in the Figure 19. The rank 6 processed specimen stirred zone shows the fine grains having medium level clustering of intermetallic compounds composed, due to lower rotational speed and maximum of traverse speed. The stirred zone micrographs of rank 6 with lower and higher magnification are presented in Figure 20. Similarly, the HAZ micrograph of the rank 6 specimen is exhibited in the Figure 21. The rank 9 processed specimen stirred zone displays the fine grains having high agglomeration of intermetallic compounds produced, due to maximum of axial load and moderate rotational speed and traverse speed [23]. The stirred zone micrographs of rank 9 with lower and higher magnification are presented in Figure 22. The HAZ micrograph of the rank 9 specimen is exhibited in the Figure 23.

The processed zone with addition of ceramic particle (Cr_3C_2) composites produced fine grains with scattered distribution of small ceramic particles. This was more evident for microstructure of processed specimen with fine grained primary aluminium grains with precipitated eutectic constituents of Mg_2Si constituents [24].

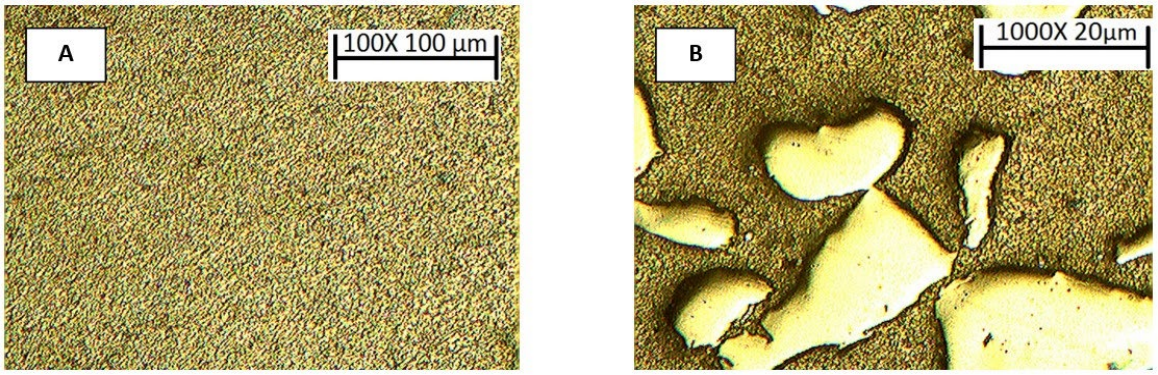

Figure 16. Stirred Zones of Rank 1 (A) At lower Magnification (100X) and (B) At higher magnification (1000X) with presence of ceramic particles.

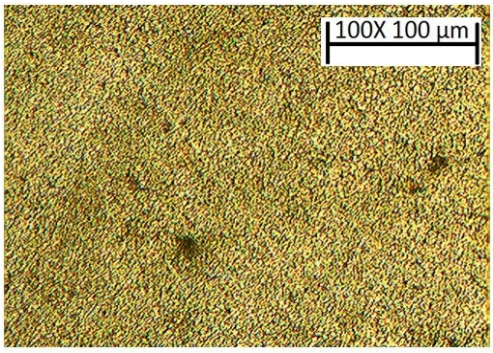

Figure 17. HAZ of Rank 1

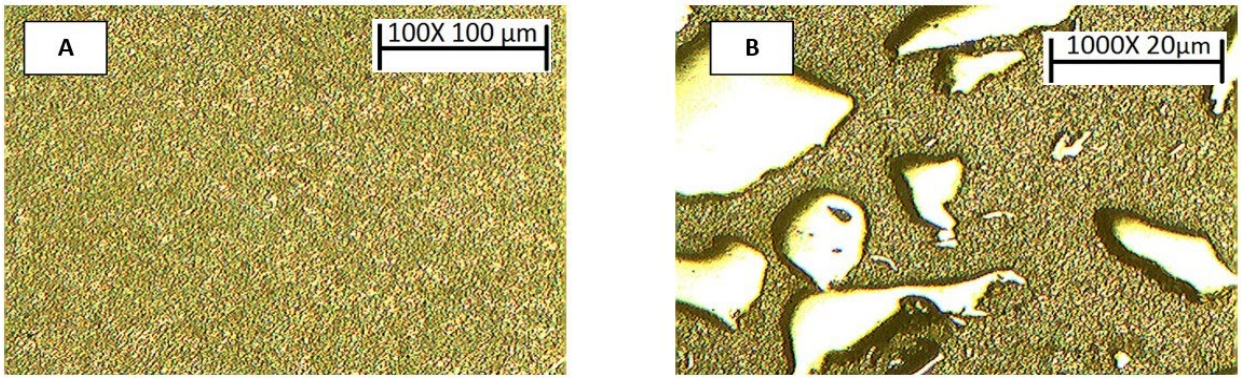

Figure 18. Stirred Zones of Rank 3 (A) At lower Magnification (100X) and (B) At higher magnification (1000X) with presence of ceramic particles.

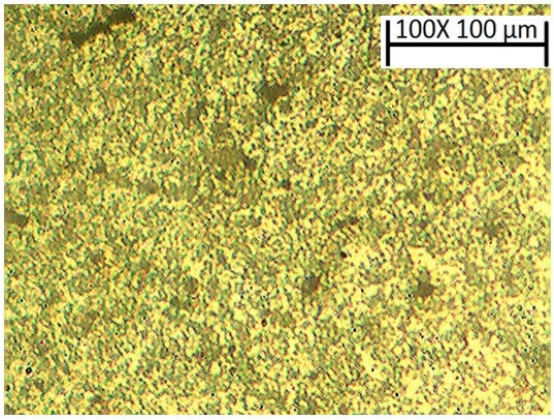

Figure 19. HAZ of Rank 3.

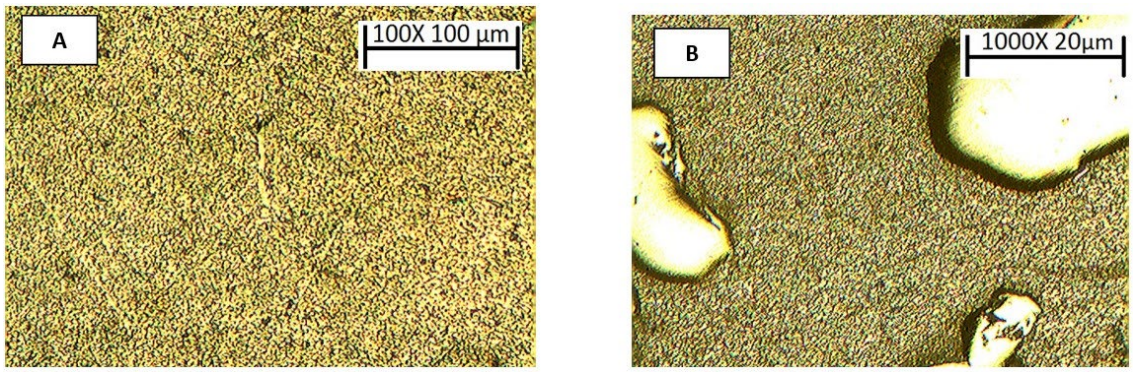

Figure 20. Stirred Zones of Rank 6 (A) At lower Magnification (100X) and (B) At higher magnification (1000X) with presence of ceramic particles.

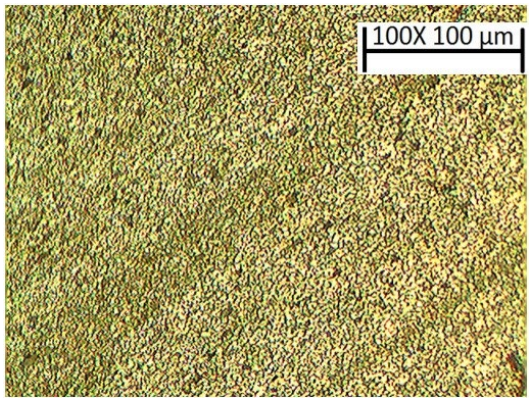

Figure 21. HAZ of Rank 6.

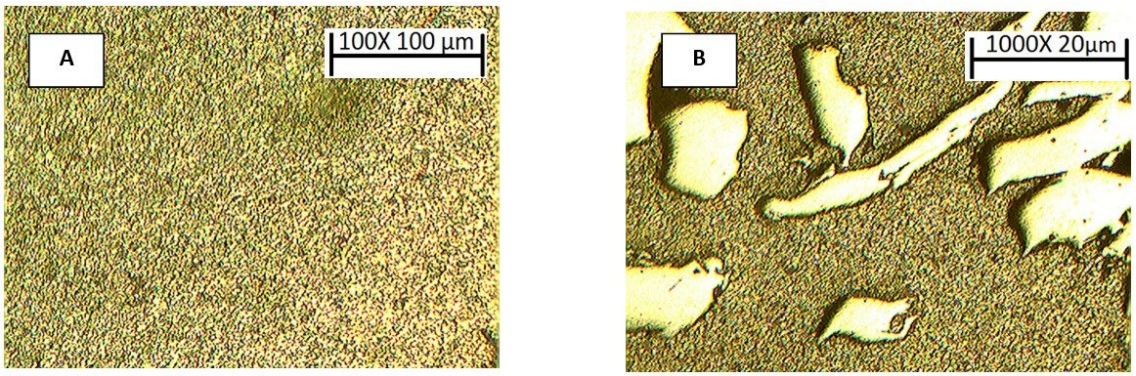

Figure 22. Stirred Zones of Rank 9 (A) At lower Magnification (100X) and (B) At higher magnification (1000X) with presence of ceramic particles.

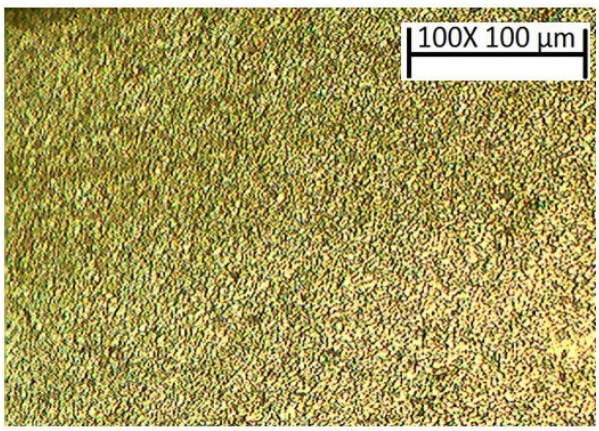

Figure 23. HAZ of Rank 9.

3.10. FESEM and EDS studies on optimal processed specimen

Field emission scanning electron was used to attain maximum GRG rank 1 by the processing parameters of 1200 rpm of tool spinning speed, 45 mm/min of tool traverse speed and 5 kN of axial load. To identify the ceramic particle presence electron dispersion spectroscopy was used. This specimen presented better mechanical properties and the ceramic particulate was well scattered and homogeneously distributed in the interface region as observed by OM structure at lower magnification. The presence of chromium carbide elements in the processed region can be identified using EDS. Figure 24 exhibits the FESEM of processed specimen of Rank 1 optimal parameters with 1000X magnification. Figure 25 shows the EDS of rank 1 parameter, indicating a possible evidence for chromium carbide presence. Table 12 shows the chemical composition after the processing by EDS analysis. Aluminium plays a major contribution subsequently, chromium and carbide occurs the second major contribution.

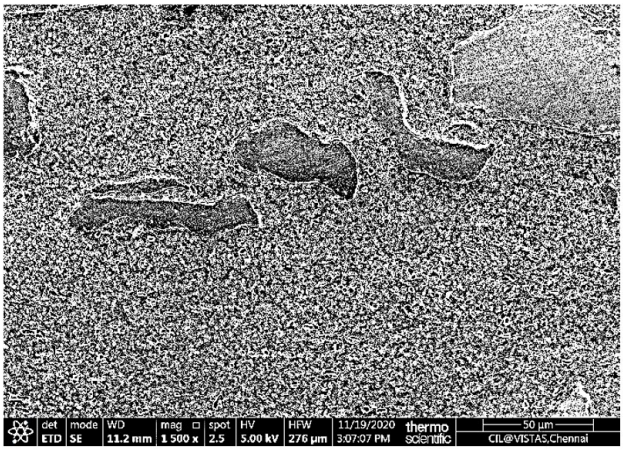

Figure 24. FESEM of Rank 1 specimens.

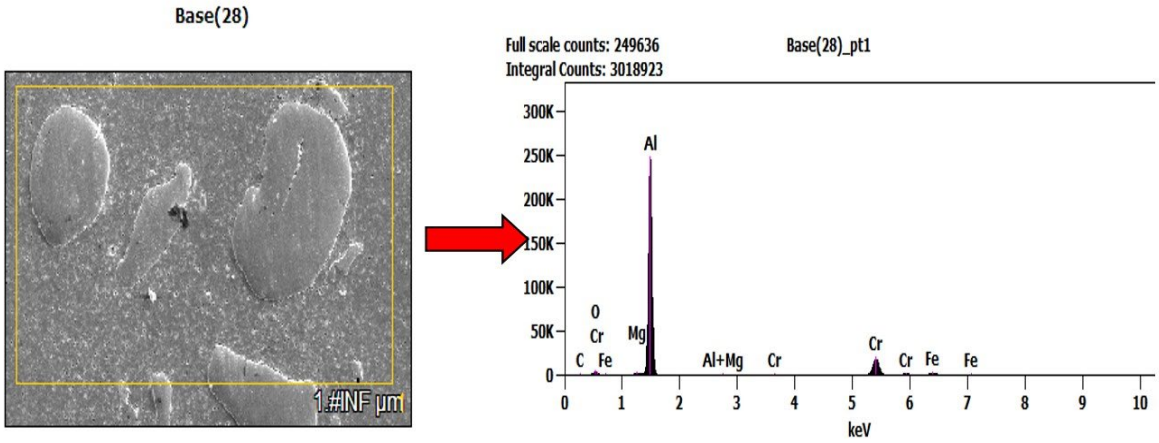

Figure 25. EDS analysis of Rank 1 specimens with FESEM image.

Table 12 Processed Element values of Rank 1 specimen.

Elements	C	O	Mg	Al	Cr	Fe
weight %	1.99	4.50	0.32	69.79	18.40	5.00

3.11. Corrosion resistance of optimum processed specimen

The corrosion behaviors of friction stir processed optimal specimens were examined by the Potentio-dynamic polarization technique. Based on the GRA, optimal process parameters are observed by using Taguchi technique and its GRA rank allotted the optimal position. So that, the rank number 1, 3, 6, and 9 related specimens were submitted to the potentio dynamic polarization test. The polarization curves of specimens Rank 1: 1200/45/5, Rank 3: 1000/60/5, Rank 6: 800/60/7 and Rank 9: 1000/45/7 with percentage of 3.5 NaCl solution are shown in Figure 26-29. The Tafel extrapolation is used to analyze the corrosion current densities of the friction stir processed AA6082 in optimal condition and base metal. The corrosion results are exhibited in Table 13.

Table 13. Corrosion results of Friction stir processed specimen AA6082 / Cr_3C_2.

Specimens	Rest potential (mV)	Corrosion Current (mA/cm^2)	Corrosion rate (mils/year)	Corrosion rate (mm/year)
Rank 1	-782.68	0.1285	55.11	1.399
Rank 3	-791.22	0.2027	86.916	2.20
Rank 6	-803.41	0.4891	209.73	5.3271
Rank 9	-793.3	0.9334	400.19	10.614
Base Metal	-787.56	0.2179	93.441	2.373

The rank 1 and 3 indicates the higher corrosion resistance with smaller current densities than rank 6 and 9. The distribution of ceramic particles is homogeneous in processed AA6082 specimen (rank 1 and 3). Normally, the strengthen particle in the processed aluminium alloy maintains the corrosion rate [25]. In rank 6 and 9 specimens posses the lower corrosion resistance because bonding between the AA6082 and strengthen particle was inadequate [26]. Also rank 1 and 3 processed specimen achieved higher corrosion resistance than the unprocessed base metal. It revealed that the optimal process parameter is a major reason for increasing the corrosion resistance, since the processed specimen (1 and 3) combined higher rotational speed and minimum axial load [27,28]. Also, the axial load has strong contribution on GRG output as shown in the ANOVA results, suggesting an evidence for producing the better outcomes.

The main factor for improving the corrosion resistance of AA6082 processed specimens is the presence of lower grain size in the grain boundaries and the dispersion of ceramic particles. The lower corrosion resistance of AA6082 processed samples is the presence of marginal grain size in the grain boundaries and the agglomerated of ceramic particles in the processed zone area. The FESEM images ensures homogenous dispersion of ceramic particles and also refined grains. The same is having good agreement with past studies in the literature.

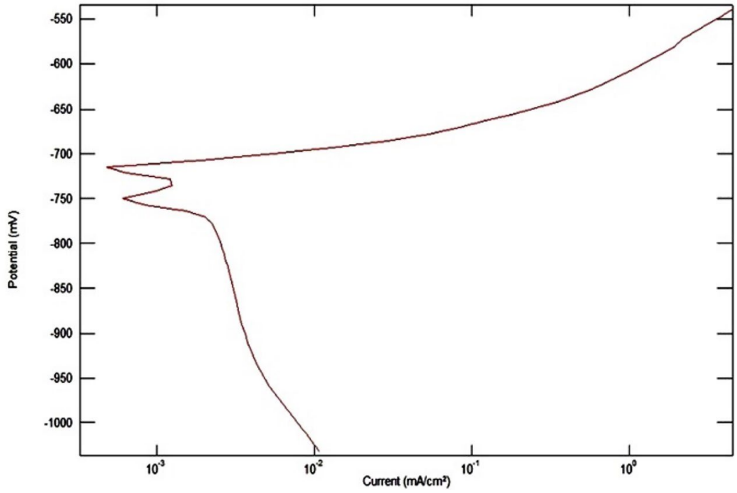

Figure 26. (Rank 1)1200 rpm rotational tool of the speed, 45 mm/min traverse speed and 5 kN axial load.

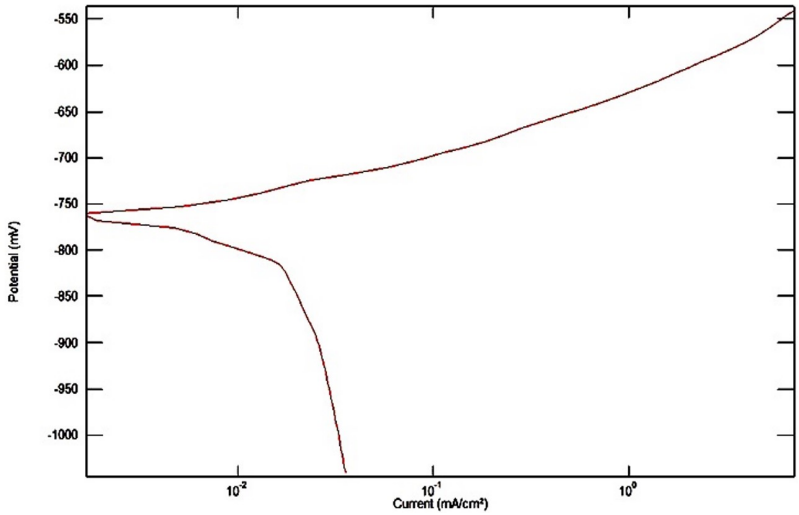

Figure 27. (Rank 3)1000 rpm rotational tool of the speed, 60 mm/min traverse speed and 5 kN axial load.

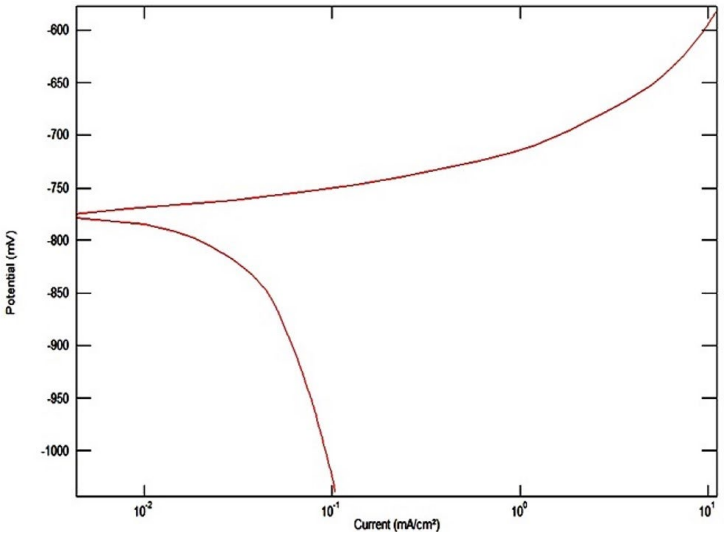

Figure 28. (Rank 6) 800 rpm rotational tool of the speed, 60 mm/min traverse speed and 7 kN axial load.

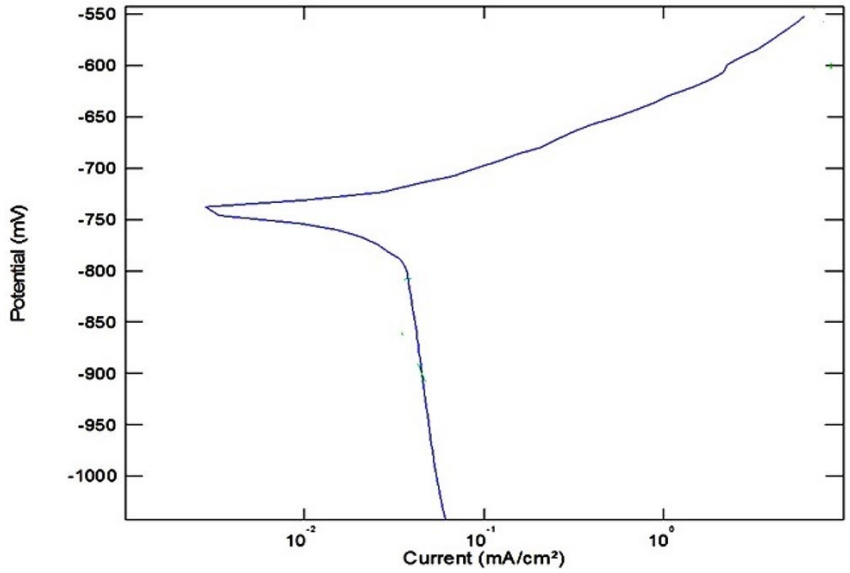

Figure 29. (Rank 9)1000 rpm rotational tool of the speed, 45 mm/min traverse speed and 7 kN axial load.

4. Conclusion

In this study, aluminium alloy AA6082 strengthened with chromium carbide particles was successfully fabricated by FSP to investigate influence of various process parameters as per Taguchi's L9 Orthogonal array. Microstructures, Mechanical properties and corrosion behavior were studied on the friction stir processed zones to understand the effect of adding chromium carbide particles in the base metal. The optimized multi performances for FSP of AA6082 were approached by Taguchi L9 with grey relational analysis. The FSP input parameters (RTS, TS and AL) on multiple output responses (TS and PSH) were studied. The following points were found as valid to represent as the concluding remarks of the present study.

- The optimized multi performances for FSP of AA6082 were approached by Taguchi L9 with grey relational analysis. The FSP input parameters (RTS, TS and AL) on multiple output responses (TS and PSH) were studied;
- The optimal combination of FSP parameters was identified as RTS at 3rd level (1200 rpm), TSS at 2nd level (45 mm/min) and AL at 1st level (5 kN). These ranges are confirmed with investigational outcomes and better concurrence was achieved by multi-objective optimization technique through FSP method.
- Simultaneously, verification results were enhanced the responses of outcomes (TS and PSH). The tool ANOVA has shown that axial load is more significant than other input parameters with a maximum contribution of 66.1%;
- The straight threaded cylindrical tool pin profile has produced modified grains structure in the processed zones. The modified fine grains structure at processed zone enhanced the values of TS and PSH for processed specimen;

- Finally, the GRG was utilized to improve the overall performances of the FSP. The specimen prepared under optimal process parameter condition has exhibited higher corrosion resistance than the other processed specimens;
- The error percentage is only 0.1% in ANOVA analysis and the contribution of rotational transverse speed is not much influencing as the contribution percentage is only 4.3%.

Authors' contributions

RB: formal analysis, writing – original draft, methodology. GE: data curation, supervision, writing – review & editing.

References

[1] Ma Z. Friction stir processing technology: a review. Metallurgical and Materials Transactions. A, Physical Metallurgy and Materials Science. 2008;39(3):642-658. http://dx.doi.org/10.1007/s11661-007-9459-0.

[2] García-Vázquez F, Vargas-Arista B, Muñiz R, Ortiz JC, García HH, Acevedo J. The role of friction stir processing (fsp) parameters on TiC reinforced surface Al7075-T651 aluminiumalloy. Soldagem e Inspeção. 2016;21(4):508-516. http://dx.doi.org/10.1590/0104-9224/si2104.10.

[3] Ma ZY, Sharma SR, Mishra RS. Microstructural modification of as-cast Al-Si-Mg alloy by friction stir processing. Metallurgical and Materials Transactions. A, Physical Metallurgy and Materials Science. 2006;37(11):3323-3336. http://dx.doi.org/10.1007/BF02586167.

[4] Mostafa D, Hamid O, Behrouz B, Mohammad J, Mahmoud A. The effect of SiC/Al_2O_3 particles used during FSP on mechanical properties of AZ91 magnesium alloy. International Journal of Materials Research. 2014;105(4):369-374. http://dx.doi.org/10.3139/146.111025.

[5] Chanakyan C, Sivasankar S, Alagarsamy SV, Dinesh Kumar S, Sakthivelu S, Meignanamoorthy M, et al. Parametric optimization for friction stir welding with AA2024 and AA6061 aluminium alloys by ANOVA and GRG. Materials Today: Proceedings. 2020;27:707-711.

[6] Elatharasan G, Manikandan R, Karthikeyan G. Multi-response optimization of process parameters in friction stir welding of dissimilar aluminium alloys by Grey relation analysis (AA 6061-T6 & AA5083-H111). Materials Today: Proceedings.2021;37:1172-1182.

[7] Jambhale S, Kumar S, Kumar S. Multi-response optimization of friction stir spot welded joint with grey relational analysis. Materials Today: Proceedings.2020;27:1900-1908.

[8] Sahu PK, Pal S. Multi-response optimization of process parameters in friction stir welded AM20 magnesium alloy by Taguchi grey relational analysis. Journal of Magnesium and Alloys.2015;3(1):36-46. http://dx.doi.org/10.1016/j.jma.2014.12.002.

[9] Sudhagar S, Sakthivel M, Mathew PJ, Daniel SAA. A multi criteria decision making approach for process improvement in friction stir welding of aluminium alloy. Measurement.2017;108:1-8. http://dx.doi.org/10.1016/j.measurement.2017.05.023.

[10] Wakchaure KN, Thakur AG, Gadakh V, Kumar A. Multi-objective optimization of friction stir welding of aluminium alloy 6082-T6 using hybrid taguchi-grey relation analysis- ANN method. Materials Today: Proceedings.2018;5:7150-7159.

[11] Arun Babu N, Balunaik B, Ravi B, Rajkumar G. Process parameter optimization for producing AA7075/WC composites by friction stir welding. Mater Today-Proc.2018;5(9):18992-18999. http://dx.doi.org/10.1016/j.matpr.2018.06.250.

[12] Chanakyan C, Sivasankar S. Parametric advancement of numerical model to predict the mechanical properties of friction stir processed AA5052. International Journal of Rapid Manufacturing.2019;8(1/2):147-160. http://dx.doi.org/10.1504/IJRAPIDM.2019.097031.

[13] Mahmoud ERI, Ikeuchi K, Takahashi M. Fabrication of SiC particle reinforced composite on aluminium surface by friction stir processing. Science and Technology of Welding and Joining. 2008;13(7):607-618. http://dx.doi.org/10.1179/136217108X333327.

[14] Dinaharan I, Zhang S, Chen G, Shi Q. Development of titanium particulate reinforced AZ31 magnesium matrix composites via friction stir processing. Journal of Alloys and Compounds. 2020;820:153071. http://dx.doi.org/10.1016/j.jallcom.2019.153071.

[15] Barati M, Abbasi M, Abedini M. The effects of friction stir processing and friction stir vibration processing on mechanical, wear and corrosion characteristics of Al6061/SiO2 surface composite. Journal of Manufacturing Processes. 2019;45:491-497. http://dx.doi.org/10.1016/j.jmapro.2019.07.034.

[16] Mahajan M, Rajpoot S, Pandey OP. In-situ synthesis of chromium carbide (Cr3C2) nanopowders by chemical reduction route. International Journal of Refractory Metals and Hard Materials, 2015;50:113-119. https://doi.org/10.1016/j.ijrmhm.2014.12.010.

[17] Yang Y, Yu J, Zhao H, Zhang H, Zhao P, Li Y, et al. Cr_7C_3: a potential antioxidant for low carbon MgO–C refractories. Ceramics International. 2020;46(12):19743-19751. http://dx.doi.org/10.1016/j.ceramint.2020.04.298.

[18] Sahu S, Patel SK, Shekhar S. The effect of grain boundary structure on chromium carbide precipitation in alloy 600. Materials Chemistry and Physics. 2021;260:124145. http://dx.doi.org/10.1016/j.matchemphys.2020.124145.

[19] Chanakyan C, Babu PD, Jenarthanan MP, Jagathesh K. An experimental investigation on mechanical properties and microstructure of friction stir welding of AA5052. Applied Mechanics and Materials. 2014;592–594:48-52. http://dx.doi.org/10.4028/www.scientific.net/AMM.592-594.48.

[20] Liu S, Jeffrey F. The role and position of grey system theory in science development. Journal of Grey System. 1997;4:351-356.

[21] Kumar S, Kumar S. Multi-response optimization of process parameters for friction stir welding of joining dissimilar Al alloys by gray relation analysis and Taguchi method. Journal of the Brazilian Society of Mechanical Sciences and Engineering. 2015;37(2):665-674. http://dx.doi.org/10.1007/s40430-014-0195-2.

[22] Lal S, Kumar S, Khan ZA, Siddiquee AN. Multi-response optimization of wire electrical discharge machining process parameters for Al7075/Al2O3/SiC hybrid composite using Taguchi-based grey relational analysis. Proceedings of the Institution of Mechanical Engineers, Part B: Journal of Engineering Manufacture. 2015;229(2):229-237. http://dx.doi.org/10.1177/0954405414526382.

[23] Dieter GE, Bacon D. Mechanical metallurgy. London: McGraw-Hill; 1988. p. 184-193.

[24] Kansal HK, Singh S, Kumar P. Parametric optimization of powder mixed electrical discharge machining by response surface methodology. Journal of Materials Processing Technology. 2005;169(3):427-436. http://dx.doi.org/10.1016/j.jmatprotec.2005.03.028.

[25] Barmouz M, Kazem M, Givi B, Kazem M, Jafari J. Influence of tool pin profile on the microstructure and mechanical behavior of Cu/SiC metal matrix composites produced by friction stir processing. Advanced Materials Research. 2011;154-155:1761-1766. http://dx.doi.org/10.4028/www.scientific.net/AMR.154-155.1761.

[26] Barmouz M, BesharatiGivi MK, Seyfi J. On the role of processing parameters in producing Cu/SiC metal matrix composites via friction stir processing: investigating microstructure, microhardness, wear and tensile behavior. Materials Characterization. 2011;62(1):108-117. http://dx.doi.org/10.1016/j.matchar.2010.11.005.

[27] El-Menshawy K, El-Sayed A-WA, El-Bedawy ME, Ahmed HA, El-Raghy SM. Effect of aging time at low aging temperatures on the corrosion of aluminium alloy 6061. Corrosion Science. 2012;54:167-173. http://dx.doi.org/10.1016/j.corsci.2011.09.011.

[28] Nam ND, Dai LT, Mathesh M, Bian MZ, Thu VTH. Role of friction stir welding – Traveling speed in enhancing the corrosion resistance of aluminiumalloy. Materials Chemistry and Physics. 2016;173:7-11. http://dx.doi.org/10.1016/j.matchemphys.2016.02.004.